Impacts of dynamic capillary pressure effects in supercritical CO2-Water flow: Experiments and numerical simulations

Impacts of dynamic capillary pressure effects in supercritical CO_2-Water flow:Experiments and numerical simulations

Luqman K. Abidoye[$], Diganta B. Das*

Chemical Engineering Department, Loughborough University, Loughborough, Leicestershire, LE11 3TU, United Kingdom

[$]Current address: Department of Civil Engineering, Osun State University, Osogbo, Nigeria

*Corresponding author (Email: D.B.Das@lboro.ac.uk; Phone: 0044 1509 222509)

ABSTRACT

Contrary to report that dynamic capillary pressure effect was insignificant in the supercritical CO_2-water ($scCO_2$-water) flow system, this work found the effect to be considerable in the displacement of water or brine by injected $scCO_2$in the geological carbon sequestration, especially prior to the attainment of equilibrium in the system. Series of controlled laboratory scale experimental measurements and numerical simulations of the dynamic capillary pressure effect and its magnitude (dynamic coefficient, τ) for supercritical CO_2-water($scCO_2$-water) system are reported inunconsolidated silica sand. Novel measurement technique has been developed to achieve this purpose, by applying the concept of two-phase flow system in the context of geological carbon sequestration. This work considers the injection of $scCO_2$ into storage aquifer as a two-phase flow system, where the CO_2 displaces the resident fluid (brine or water). Using a high-pressure and high-temperature experimental rig, capillary pressure–saturation relationships (P^c-S) for this flow system and the saturation rate dependencies of theP^c-S relationships (quantified by dynamic coefficient, τ), known as dynamic capillary pressure effect were determined. This τ was previously unreported for $scCO_2$-water system. In $scCO_2$-water flow system, τ ranges from 2 x10^5 to 6 x10^5 Pa s at high water saturation and 1.3 x 10^6 to 8 x10^6Pa saround the irreducible saturation. τ increases with rising temperature but decreases with increase in porous medium permeability. Numerically determined τ-S relationships compare well with the corresponding experimental results for wide range of water saturation.The implication was that

water saturation of the porous media will be considerably underestimated, if the dynamic capillary pressure effectwas ignored in the characterization of the $scCO_2$-water flow system , i.e., if only equilibrium $P_c$relationship was used.

Keywords: Dynamic capillary pressure effects, dynamic coefficient, supercritical CO_2, geological carbon sequestration.

1. Introduction

The problem of global warming, as a result of the emissions of greenhouse gases, is of international concern. Capturing these gases (especially CO_2) from the emission sources and storing them in geological media, in a process known as geological carbon sequestration has been a subject of global interest with hugeinvestment and research(Petvipusit et al. 2014; Stephens 2006). Thecaptured $CO_2$is injected into geological formation, e.g. brine aquifer, at suitable depths, where subsurface temperature and pressure will maintain CO_2 at supercritical state, having higher density and viscosity to limit the CO_2mobility and buoyancy. Following the injection of supercritical CO_2 ($scCO_2$) into a geological formation, it will displace the resident brine or groundwater in the brine aquifer. This displacement occurs as a two-phase flow system(Tokunaga et al. 2013; Khudaida and Das 2014; Abidoye et al. 2014; Das et al. 2014). Similarly, two-phase flow behaviour is regularly encountered and has been widely studied in the studies of oil recovery, immiscible contaminant remediationand so on.For example, there are cases of subsurface contamination by non-aqueous phase liquids, i.e., NAPLs (e.g., oils, perchloroethylene (PCE), etc.), which are produced, and may be accidentally spilt, by various chemical process industries (CPIs). These NAPLs may remain in the subsurface for hundreds of years and pose environmental threats worldwide(Das et al. 2007; Chandrappa and Das 2014).Like the above two-phase flow systems, studying and understanding the flow of $scCO_2$-brine/water in the subsurface involve experiments, modelling and simulation of the system and processes (Abidoye et al. 2014; Khudaida and Das 2014; Das et al. 2014). Doing this requires the determination and analysis of capillary pressure (P^c) as a function of saturation of wetting (S) or non-wetting (S_{nw}) phases. P^c and S are key variables of importance in modelling the two-phase flow processes taking place in the subsurface (Aggelopoulos and Tsakiroglou 2008).

Traditionally, the P^c-S relationships of the two-phase systems are studied under the equilibrium or quasi-static condition(see, e.g., Jennings 1987; Donaldson et al. 1969; Donaldson et al. 1991). Mathematically, this is achieved by the use ofa P^cfunction coupled with an extended version of Darcy's law for single-phase flow, where the P^c is defined as a function (f) of saturation as shown in equation (1).

$$P_{nw} - P_w = \quad P^{c,equ}(S) = f(S) \tag{1}$$

Where,

$P_{nw} = \text{average pressure for non} - \text{wetting phase} \left[ML^{-1}T^{-2}\right]$
$P_w = \text{average pressure for wetting phase} \left[ML^{-1}T^{-2}\right]$
$P^{c,equ} = \text{equilibrium (steady state) capillary pressure} \left[ML^{-1}T^{-2}\right]$
$S = \text{wetting phase saturation} \left[-\right]$

However, many factors have been identified which affect the above relationship. In particular, the flow rate dependence of P^c-S relationship was discussed by Kalaydjian (1992). This phenomenon was also observed by a number of other authors (see, e.g., Dullien et al. 1990; Danish and Jacquin 1983). Saturation-rate dependencies in flow properties observed during non-steady state multiphase flow are generally referred to as 'dynamic capillary pressure effect' (Hassanizadeh et al. 2002) or simply 'dynamic effect'. The dynamic P^c effect has been the subjects of many publications (see, e.g., Barenblattet al. 2003; Joekar-Niasar et al. 2010; Stauffer 1978; Kalaydjian 1992; Wildenschild et al. 2001; Hassanizadeh et al. 2002; O'Carroll et al. 2005; Oung et al. 2005; Camps-Roach et al. 2010; Sakaki et al. 2010; Goel and O'Carroll 2011; Das and Mirzaei 2012; Diamantopoulos and Durner 2012; Das et al. 2014; Khudaida and Das 2014). Some of these investigators (e.g., Stauffer 1978; Kalaydjian 1992; Hassanizadeh and Gray 1993) have proposed a modification of the P^c-S function to account for dynamic P^c effect in two-phase flow systems prior to the attainment of equilibrium or quasi static condition. The modification is shown in equation (2):

$$\left(P^{c,dyn} - P^{c,equ}\right)\Big|_S = -\tau\, \partial S \big/ \partial t\Big|_S \tag{2}$$

where,

96 $P^{c,dyn} = \text{dynamic capillary pressure}\ [ML^{-1}T^{-2}]$

97 $\partial S/\partial t = \text{time derivative of saturation}\ [T^{-1}]$

98 τ =dynamic coefficient [$ML^{-1}T^{-1}$]

99

100 The magnitude of τ has been related to how close or far the two-phase system is
101 from equilibrium (Das et al. 2007). Most of the works available on these relationships
102 are related to oil-water system in application to oil recovery. However, recent
103 development in climate change mitigation techniques and the subsequent practice of
104 the geological carbon sequestration has brought $scCO_2$ and brine/water into focus as
105 an important two-phase system in porous media(Abidoye et al 2014; Chandrappa et
106 al. 2011). Geological storage of supercritical CO_2 generally utilises brine aquifers
107 where it is hoped that the CO_2 will remain trapped for geological time-scales (Elenius
108 and Gasda 2012). However, since the displacement by brine and migration of CO_2
109 occur in the subsurface, reliable predictions and monitoring of the fate of CO_2 require
110 understanding of the capillary behaviour of supercritical CO_2 and its dependence on
111 water saturation (Tokunaga et al. 2013).The pathway-dependence of phase
112 displacement in two-phase flow in the porous media has led to the investigation of
113 hysteretic dynamic capillarity effect on P^c-S relationship (Zhuang et al. 2017) while
114 effect of acoustic excitation on the dynamic P^c-S was undertaken by Lo et al. (2017)
115
116 Despite the above efforts in the literature, the saturation rate dependence of the P^c-S
117 relationship for $scCO_2$-water system has not been fully understood. Currently, no
118 experimental investigations have been reported for the τ-S behaviour in relation to
119 geological sequestration of CO_2. Furthermore, no experimental reports are available
120 on the temperature dependency of τ-S relationship for $scCO_2$-water-porous media
121 system. In reality, prior to the attainment of equilibrium, the unsteady state or
122 dynamic condition resulting from the injection of the $scCO_2$ into the host media
123 cannot be described by the traditional P^c-S relation. Thus, it is imperative to
124 investigate the presence of dynamic effect in the P^c-S relationship for $scCO_2$-water
125 system, using the new relation in equation (2). Authors of a number of works on
126 dynamic P^c effect (see, e.g., Juanes 2008; Camps-Roach et al. 2010; Goel and
127 O'Carroll 2011) called for an inclusion of τ in the modelling and simulation of
128 geological sequestration system. Using numerical simulations, Khudaida and Das

(2014) as well as Das et al. (2014)report the importance of dynamic P^c effect in the P^c-S relationship for $scCO_2$-water system. However, no direct experimental study to confirm the presence of dynamic P^c effect has been reported for $scCO_2$-water system. In a related investigation, Wang and Tokunaga (2015) expressed that the drainage P^c-S relationship controlled the distribution of CO_2 and brine in the pore space during injection. They also acknowledge that the distribution varies with distances from the well. But, the impact of dynamic effect on the P^c-S relationship was not investigated by these authors.

In this work experimental and numerical investigation techniques were used to study the dynamic P^c effect in the $scCO_2$-water flow system in a porous media. The novelty of this work included the first-ever determination of dynamic effect for supercritical CO_2-water system. This is different from other publications which determine the dynamic effect under ambient conditions. Secondly, the method of measurement in this work was also novel by including design of the sensor holder for the $ScCO_2$-water system together with the water-resistant membrane and other materials used to prevent water infiltration into the sensor chamber while allowing CO_2.Effects of temperature, media permeability and surfactants on the dynamic Pc effects were determined. Finally, this work discusses the inherent error in the estimation of fluid saturation of the porous media, as a result of ignoring dynamic capillary pressure effect.

2. Methodology

2.1 Fluids and Porous Materials

High purity (99%) CO_2 was used in this work to displace water from water-saturated porous domain. The porous medium used in this work was composed of silica sand categorised as fine-grained (CH30) or coarse-grained (DA 14/25) sand samples. The terms fine and coarse are relative to indicate the different in sizes of the snad particles. Simillar terminologies were used in previous publications (Abidoye and Das 2014; Das et al. 2014). They were obtained from Minerals Marketing Limited (Buxton, UK). The physical and chemical properties of the samples are listed in Table 1. Before use, they were pre-treated by washing in deionised water and dried for at least 24 hours in open air at ambient temperature. To ensure uniform packing

of the porous domain in every experiment, the sand was poured through sieve into the experimental cell which initially contains water. The surfactant used was alkylpolyglucosides obtained from BASF (Ludwigshafen, Germany).

Table 1: Fluid and Material Properties

Materials Properties	**Fine silica sand (CH30)**	**Coarse silica sand (DA14/25)**	**Fluids Properties**			
			Pressure: 80.5bar Temperature: 40°C		**Pressure: 80.5bar Temperature: 50°C**	
			CO_2[a]	**Water[b]**	**CO_2[a]**	**Water[b]**
Permeability, K (m^2)	5.66 x 10^{-11}	3.65 x 10^{-10}	-	-	-	-
Porosity, ϕ (-)	0.37	0.38	-	-	-	-
Density (kg/m^3)	2660[d]	2740 [d]	288	996	223	992
Average particle diameter, D_p(μm)	482.4	946.1	-	-	-	-
Viscosity, μ (Pa s)	-	-	23 x10^{-6}	654x10^{-6}	21x10^{-6}	548x10^{-6}
SiO_2 (%)[c]	99[b]	99[b]	-	-	-	-
Entry pressure, P^d(Nm^{-1})	660	431	-	-	-	-
Pore size distribution index, λ (-)	3.86	3.50	-	-	-	-
Residual water saturation, S_{rw}(-)	0.11	0.09	-	-	-	-

[a]http://www.peacesoftware.de/einigewerte/co2_e.html (accessed March , 2019)

[b]http://www.peacesoftware.de/einigewerte/wasser_dampf_e.html (accessed March, 2019)

[c]www.sibelco.co.uk (accessed March , 2019)

[d] Density was determined by gas pycnometer (AccuPyc II 1340, Micromeritics, USA)

2.2 Sample holder for porous mediaand instruments

The sample holder is a steel cell domain designed to hold pressure transducers at its centre. The domain has the dimension of 4 cm height by 10 cm diameter. The domain has ports at its centre, where the phase pressures were measured with the aid of the pressure transducers (PTs). The PTs' cables were connected to a datalogger (Compact DAQ chassis, National Instrument, Newbury, UK), which collects the data readings from the PTs for onward processing in the computer. The data from the PTs were processed in the computer using LABVIEW (National Instruments, Newbury, UK). For measuring water phase pressure, the pressure transducers are housed in a fabricated steel holder with sintered metal at the inner face. The sintered metal was overlaid with a hydrophilic nylon membrane with a pore size of 0.1µm (Porvair Filtration Group Ltd, Hampshire, UK). On top of the hydrophilic membrane was placed a 5mm thick Vyon hydrophilic filter (Porvair Filtration Group Ltd, Hampshire, UK) previously soaked in a beaker of water and vacuumed for at least 24 hours. An open steel cap was then corked on top of the holder to hold the filter and the membrane in tight contact with the sintered metal disc and, also seal off any unwanted tiny sideways, where fluid might preferentially follow. The open space in the steel cap was filled with cotton wool previously soaked in water in order to avoid pooling of fluid in the small hollow space.

Similarly, to measure the $scCO_2$ phase pressure, 1µm hydrophobic polytetrafluoroethylene, PTFE membranes (Porvair Filtration Group Ltd., Hampshire, UK) was used together with the thick hydrophobic filter (Porex Technologies, GmbH, Germany) and cotton wool. In this case, the cotton wool and the filter were soaked in silicone oil and vacuumed for at least 24 hrs. The assembly was done in the same way as for the water phase pressure measurement. CO_2 is reportedto be soluble in silicone oil (Wedlake and Robinson, 1979) and can thus be used to distinguish the phases as water is known to be insoluble in the oil. To ensure quick response of the pressure transducer, the gap between the sintered metal disc and the face of the pressure transducer at the base of the holder was made as small as possible.

In situ wetting phase saturation (S) measurement was done with three-pin time domain reflectometry probes (TDR). The pins were locally fabricated to perform under high temperature and pressure applicable to this work. They were insulated in the region of contact with the steel domain to avoid interference with the signal. The TDR probe cable

183 was plugged into the multiplexer (Campbell Scientific Ltd, Shepshed, UK). This was
184 connected to the time-domain reflectometer-TDR100 (Campbell Scientific Ltd, Shepshed,
185 UK) where the impulses were generated. This was then connected to CR10X datalogger
186 (Campbell Scientific Ltd, Shepshed, UK) for automatic recording of the data generated. At
187 the start of the experiment, the TDR probes were calibrated to generate the offset and
188 multiplier following the Campbell Scientific Instruction manual for such. Similarly, the PTs
189 were calibrated using Druck 610 Calibrator (Druck Limited, Leicester, UK). To sync the
190 readings from the LABVIEW with readings from the Loggernet of the CR10X datalogger,
191 an interval of 10s was set for data acquisition in both devices. The calibration results were
192 fitted with a polynomial function and applied in programming the respective software.
193 Further readings of water saturation were obtained from water outflow collected in a
194 graduated glass cylinder placed on an accurate weighing balance which was connected to
195 the computer and data logged in real time by the weighing balance software (A&D
196 Company Limited, San Jose, USA). For accuracy of outflow volume readings, the dead
197 volume in the steel tube upstream of the sample holder was subtracted from the actual
198 weighing balance reading. Figure 1 is a schematic diagram of the experimental set up. The
199 figure illustrates the domain size, the configurations of the PTs as well as the TDR probes.
200
201 Observations of the responses of the sensors - TDRs and the PTs, to change in system
202 conditions (e.g., change in water saturation, in the case of TDR, and the change in
203 pressure, in the case of PTs) did not reveal any measurable lag in their response. The
204 sensors responded well to changing conditions during the calibration as well as the actual
205 experiments and thus would not affect the readings in this (Hou et al. 2012). The
206 experimental rig was located in a heating cabinet having electric heaters to regulate the
207 system temperature. The instrument used for the temperature regulation was PID
208 temperature controller (West Control Solutions, Brighton, UK).
209
210 The sample holder has stainless steel end-pieces at the top and bottom. The top end
211 piece of the sample holder was connected to the supercritical fluid pump via a steel tube.
212 Similarly, the bottom end piece was connected to the outflow bottle on an electronic
213 weighing balance via backpressure regulator (BPR) (see, Figure 1). The $scCO_2$isinjected
214 via the upstream tube and the downstream tube serves as the outlet for water. The inner
215 part of the bottom end piece was laid with hydrophilic membrane to minimise outflow of
216 $scCO_2$ while hydrophobic membrane was fitted to the top end piece to prevent escape of
217 water into the CO_2pump. For fine control of outflow, metering valve (Swagelok, Kings

Langley, UK) was located at the outflow line. Following the metering valve is a precision back pressure regulator, BPR (Equilibar, Fletcher, NC, USA) that keeps the system at the minimum set pressure. The back-pressure regulator (BPR) is a dome loaded type, using PTFE-glass materials as diaphragm and was loaded with nitrogen gas (BOC Industrial Gases, Leicester, UK) from a cylinder with appropriate single-stage regulator (Gas-Arc Group Ltd, Norfolk, UK).Nitrogen gas was used in the experiments to impose a set pressure on the diaphragm of the BPRto counteract the gas pressure set on the supercritical fluid pump, so as to ensure stability in the system.

2.3 Dynamic and Equilibrium Experiments

At the start of the experiment, the experimental rig was set up from bottom upward. After placing the sample holder on the bottom end piece (base cover), small amount of water was poured into the cell to a certain position followed by pouring of sand through a metal sieve of appropriate size to ensure uniform sand packing and minimise air trap. Equal amount of sand (500g) was used in all cases. Then, the top end piece with the hydrophobic membrane was put in position. At this stage, all valves remained closed except V-4 (see, Figure 1) via which deionised water was passed into the sample holder and pressurised from the water tank using hand pump up to the experimental set pressure (monitored from the pressure gauge located next to the hand pump). At high pressure, all air present in the tubing and in the sand was considered dissolved (Plug and Bruining, 2007). After the supply of water into the sand-filled sample holder, valve, V-4, was then closed leaving the sample holder and water at set pressure. CO_2 used in this work was obtained from BOC industrial gases (Leicester, UK) at 99.9% purity. The supercritical fluid pump 260D model (Teledyne Isco, Lincoln, USA) was filled with liquid CO_2 from the CO_2 cylinder by opening of the valve, V-1 and setting the pump on refill mode. After filling the pump volume, the valve, V-1, was closed and the supercritical fluid pump was set at the experimental pressure. This procedure filled CO_2 to the tubing from the exit of the supercritical fluid pump up to the valve, V-2, which serves as the interface between water and CO_2. Before the start of the experiment, this valve was opened to allow pre-equilibration of water and CO_2, i.e., dissolution of CO_2 in water without any displacement of water by CO_2. Sufficient time was also allowed for temperature and pressure equilibration before opening the outlet valve (V-6) for the displacement of water to begin.

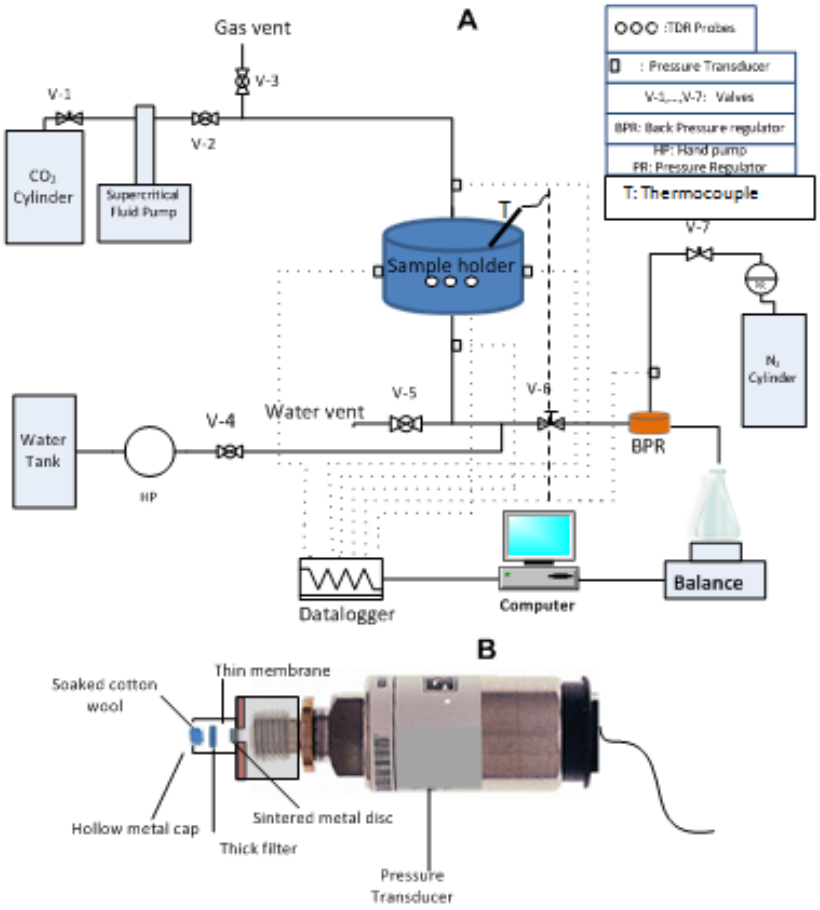

Figure 1: (A) High pressure experimental set-up for the $scCO_2$-water system (B) Configuration of the phase pressure measurement system.

For the dynamic displacement of water by $scCO_2$, the BPR was set at constant pressure condition, i.e., 80bar while the supercritical fluid pump was set at 50kPa higher pressure, i.e., 80.5bar. When there was equilibrium in the system temperature, monitored on the heating controller and there was equilibrium in the pressure set on the supercritical fluid and the BPR, valve V-2, was opened for equilibration of water and CO_2before the displacement of the water by CO_2 began. While the TDR probes give the readings of change in the in-situ water saturation, additional readings were recorded by the weighing balance from the water outflow. There was good agreement between these two readings while the dead volume was subtracted. Some sets of the experiments were repeated two or three times to allow for repeatability check and statistical analysis.

The equilibrium or quasi-static experiments were conducted by using single-pump gradient program of the supercritical fluid pump 260D model (Teledyne Isco, Lincoln, USA). This program allows stepwise, time-controlled pressurisation of the supercritical fluid. To

achieve this, the supercritical fluid pump and the back-pressure regulator were set at the same constant pressure, i.e., 80bar, following similar arrangements as described above. Then, the supercritical fluid pump was put in gradient program mode and raised at 0.5 kPa every hour. This is considered as quasi-static or equilibrium displacement since the flow proceeded slowly at each step. This continued until there was no appreciable change in the water outflow measured on the balance or when continuous gas breakthrough occurred. Experiments in which the CO_2 front was unstable was characterised with gas breakthrough in the midst of the drainage. Such results were discarded. The highest P^c values chosen in this work typically represents when we do not see changes in the water saturation.

The quasi static measurement took place over an average time of about 3 days (72hrs). The dynamic measurement took place for average time of about 10-12hrs. As for the measuring intervals of pressure sensors and TDR, they continue to measure and transmit the recorded data through CR10X data logger into the desktop memory at every twenty seconds under quasi static conditions

2.4 Numerical Simulation

In order to further understand dynamic P^c effects for $scCO_2$/water flow in porous domain, numerical simulation was conducted using the simulator, *Subsurface Transport Over Multiple Phases* (STOMP).The code is developed by the Pacific Northwest National Laboratory, US (www.pnl.gov). The simulator is capable of simulating different modes of multiphase flow and multi-component transport in porous media. In this work, the CO_2-Wateroperational mode (STOMP-CO_2) is used to simulate the dynamic and quasi-static two-phase flow behaviour.STOMP-CO_2 solves the conservation equations (partial differential) for component mass (i.e., water, CO_2) on a structured orthogonal grid(White et al. 2012). The partial differential equations were solved numerically. To solve these conservation equations, they are first converted to algebraic form using the integral finite difference approach applied to structured orthogonal grids and Euler- backward time differences (Versteeg and Malalasekera 1995; Patankar 1980). The resulting algebraic equations are closed through a series of constitutive equations. Newton-Raphson iteration is used to resolve the nonlinearities in the system of conservation equations and constitutive equations (White et al. 2012). Many authors have successfully used STOMP to simulate CO_2-Water (see, e.g., Das et al. 2014; Khudaida and Das 2014) and Oil-Water

(e.g., Das et al. 2007; Das and Mirzaei 2012; Ataie-Ashtiani et al. 2001) flow in porous media.

The results from the simulations also serve as comparison to the experimental results. Two-phase flow in coarse and fine silica sand samples were modelled under quasi-static and dynamic conditions. The boundary conditions, model governing equations, and the nodal configurations of domain geometry for the simulation are expressed in Tables 2, 3, and 4, respectively. The porous media properties used for the simulation remained as listed in Table 1. The simulations of the dynamic and quasi static displacements follow similar procedures as described in detail byDas et al. (2014) and Mirzaei and Das (2007). The CO_2 property data table is stored in a data file that was included in the simulation file. It enables interpolation of CO_2 property during the initialization stage of the simulation (White et al. 2012). To obtain the property of the CO_2 at a particular condition, the temperature and pressure of interest are specified in the simulation file. Two different temperatures, namely, 40 and 50^oC, but the same pressure (see, Table 2) were used in the simulations.

Table 2: Boundary conditions for different displacement cases used in the simulation

		Top Boundary		**Bottom Boundary**	
Displacement case	Time Duration (hr.)	Dirichlet CO_2 Pressure (Bar)	Zero Flux Water	Dirichlet Water Pressure (Bar)	Zero Flux CO2
Dynamic	3	80.5		80	
Quasi static	>40	Base pressure=80 0.005bar/step		80	

322 Table 3: Equations used for the simulation (please see full details in Das et al. (2014))*

Equation no	Description	Equations	Definition of parameters
3	Conservation of fluid mass in the two-phase flow system	$\frac{\partial}{\partial t}(\phi \rho_\gamma S_\gamma) + \nabla.(\rho_\gamma q_\gamma) = 0$ for $\gamma \equiv w, nw$	'w'= the wetting phase (water); 'nw'= the nonwetting phase (CO_2);.ϕ [-], porosity; S[-], average fluid saturation in the porous medium; $\rho[ML^{-3}]$, the fluid density; and $q[LT^{-1}]$, the fluid flux
4	Multiphase version of Darcy's law for conservation momentum	$q_i = -K_{ri}K/\mu_i[\nabla P_i + \rho_i g \nabla z]$	K $[L^2]$, the intrinsic porous media permeability; μ $[ML^{-1}T^{-1}]$, the fluid viscosity; K_r [-], the relative permeability; P $[ML^{-1}T^{-2}]$, the phase pressure; z [L], upward unit vector; g $[LT^{-2}]$, acceleration due to gravity
5	Brooks-Corey relationships for P^c(Brooks and Corey 1964)	$S_{ew} = \left(\frac{P^c}{P^d}\right)^{-\lambda}$ for $P^c \geq P^d$	S_{ew}[-]: effective saturation of the wetting phase; P^d $[ML^{-1}T^{-2}]$: entry pressure of the medium; λ[-]: pore size distribution index; S_{rw}[-]: irreducible wetting phase saturation
6		$S_{ew} = 1$ for $P^c \leq P^d$	
7		$S_{ew} = \left(\frac{S_w - S_{rw}}{1 - S_{rw}}\right)$ for $0 \leq S_{ew} \leq 1$	
8	Brooks-Corey-Burdine relationships for relative permeability (Brooks & Corey 1964; Burdine 1953)	$k_{rw} = (S_{ew})^{(2+3\lambda)/\lambda}$	
9		$k_{rnw} = (1 - S_{ew})^2(1 - S_{ew}^{(2+\lambda)/\lambda})$	

323

324 For further information about the workings of STOMP, readers are requested to read
325 publication like STOMP-CO_2 and CO_2eGuide by White et al. (2012) (Pacific Northwest
326 National Laboratory, USA).

327

Table 4: Number of nodes and nodal spacing for the domain used for numerical simulation

	Number of Nodes and Nodal Spacing		
Geometry	N x ΔR (cm)	N x ΔΘ (°)	N x ΔZ (cm)
3D Cylindrical	4 x 1.25	4 x 90	1 x 0.05, 24 x 0.1625, 1 x 0.05

Please note that R, Θ and Z are the dimensions related to radii, angle and height of the porous domain. N is the number of nodes or subdivisions in each dimension. 3D simulation was used in this work, as there are no significant differences in output, compared with 1D simulation. Also, the 3D approach enables easy comparison of the results in this work with related works in the literature (see, e.g., Das et al. (2014), Khudaida and Das (2014), etc.). Furthermore, grid sensitivity of the simulation was not conducted owing to the fact that related work by Das et al. (2014) did not find significant sensitivity to grid.

The averaging techniques employed in this work for averaging the capillary pressure (P^c) and saturation (S) are similar to those employed in the work of Abidoye and Das (2014).

2.5 Calculation of Dynamic Coefficient (τ)

Similar to the approach employed by Goel and O'Carroll (2011), Camps-Roach et al. (2010), and Sakaki et al. (2010), only one pressure, namely, 50kPa head (80.5bar from CO_2 pump, and 80bar from BPR) was applied in all the dynamic experiments. The dynamic coefficient determination was based on the P^c-S data obtained under the dynamic and quasi static conditions. The same pressure head was also applied in the numerical simulations of the dynamic flow condition.

The dynamic coefficients were determined using equation (2). To use the equation, there is a need for P^c data for the dynamic and quasi static conditions at the same water saturation (S). From the experimental and simulation data, the phase pressures (i.e., pressures for water and $scCO_2$) from the equilibrium and dynamic experiments were fitted with between 5^{th} to 10^{th} degree polynomials depending on the one with least residuals using MATLAB. The fitting equation was then used to generate capillary pressures at selected saturation within the experimental data saturation range. This procedure provides the corresponding points for the parameters in the equation (1), i.e., P_{nw} and P_w, at a particular saturation, S, for both the dynamic and equilibrium conditionsin order to get the P^c at that particular saturation. These results were then used in equation (2) to obtain $P^{c,dyn}$, and $P^{c,equ}$. Similarly, the desaturation rate data were fitted with similar order of

polynomials that give the least residuals and the desaturation data were generated for saturation values corresponding to the ones obtained for the capillary pressures. From equation (2), the division of $P^{c,dyn}$-$P^{c,equ}$ at a particular saturation by the corresponding desaturation rate gives the dynamic coefficient, τ, at that particular saturation.

We have provided only a brief discussion on the steps for the calculations of the dynamic coefficient as the calculation steps are reported in previous papers (Abidoye and Das, 2014; Goel and O'Carroll, 2011; Camps-Roach et al., 2010, Sakaki et al., 2010).

3. Results and Discussions

The results of various experimental investigations and numerical simulations of the dynamic effects in P^c-S relationship for $scCO_2$-water system in porous media, with different physical characteristics, are presented and discussed.

3.1 Experimental results

3.1.1 Dynamic effects in P^c-S relationship for supercritical CO_2-water system

The results of the investigations on dynamic P^c-S relationship are presented in this subsection. Figure 2 shows the difference between the dynamic P^c-S curve and that of the quasi static condition in silica sand sample with higher permeability (i.e., coarse sand, DA14/25) at different temperatures. The P^c-S curves help to determine entry pressures under different experimental conditions. The entry pressure signifies the pressure at which the invading phase ($scCO_2$) enters into the medium after the start of the displacement of the resident phase (water). P^c-S curve for $scCO_2$-water in coarse silica sand at 40°C is shown in Figure 2A, after the entry of CO_2 into the domain, the quasi static P^c-S profile appeared constant for most part of the water saturation values until the irreducible saturation (S_r) is approached. Close to the irreducible saturation, the P^c-S curve starts to rise steeply. For the case of dynamic curve, there is a gentle rise in the P^c-S profile with decrease in the water saturation value, even after the entry of supercritical CO_2 ($scCO_2$) into the domain. However, both categories of P^c-S curves (i.e., quasi static and dynamic) show steep rise in the values as they approach the irreducible water saturation. The quasi static P^c-S curve consistently remains lower in profile compared with the dynamic P^c-S curve. The results affirm the presence of dynamic P^c effect in the P^c-S relationship for $scCO_2$-water system in porous media. Detailed explanations of dynamic capillary pressure

effects for other fluids in porous media have been previously demonstrated (see e.g., Kalaydjian 1992; Hassanizadeh and Gray 1990; Hassanizadeh and Gray 1993; Das et al. 2007; Das and Mirzaei 2013; Abidoye and Das 2014). In Figure 2A, the P^c-S curves for $scCO_2$-water system in coarse sand at 40^{o}C are shown with the error bars. The error bars were obtained from the statistics of three different experimental measurements, using standard deviation around the mean values of the P^c, at a particular saturation. It could be seen that the deviation from the mean value is small for the large part of the water saturation values making the error bars hardly visible. The error bars become conspicuous near the irreducible water saturation. Thus, the reliability of the measurements is high for wide range of water saturation values, prior to the region of irreducible saturation.

Figure 2B shows the P^C-S curves for both dynamic and quasi static conditions at 50^{o}C in coarse sand samples while the Figure 2C shows the P^C-S curves in coarse sand sample for $scCO_2$ displacing 0.1% surfactant (alkylpolyglucosides) solution (BASF, Ludwigshafen, Germany) at 40^{o}C.It can be seen that, P^c-S curves in the case of surfactant solution also follow different paths, under different flow conditions. In addition, the curves in Figure 2C show that with surfactant solution, the P^c reduces. Therefore, in comparisons with the P^c-S curves in Figures 2 A and B, the curves in Figure 2C are much lower in P^c values at corresponding saturation. This pattern can be attributed to the lowering of interfacial tension by the presence of surfactant (Rudin et al. (1994) and Rosen (2004)). Lower interfacial tension leads to lower capillary pressure.

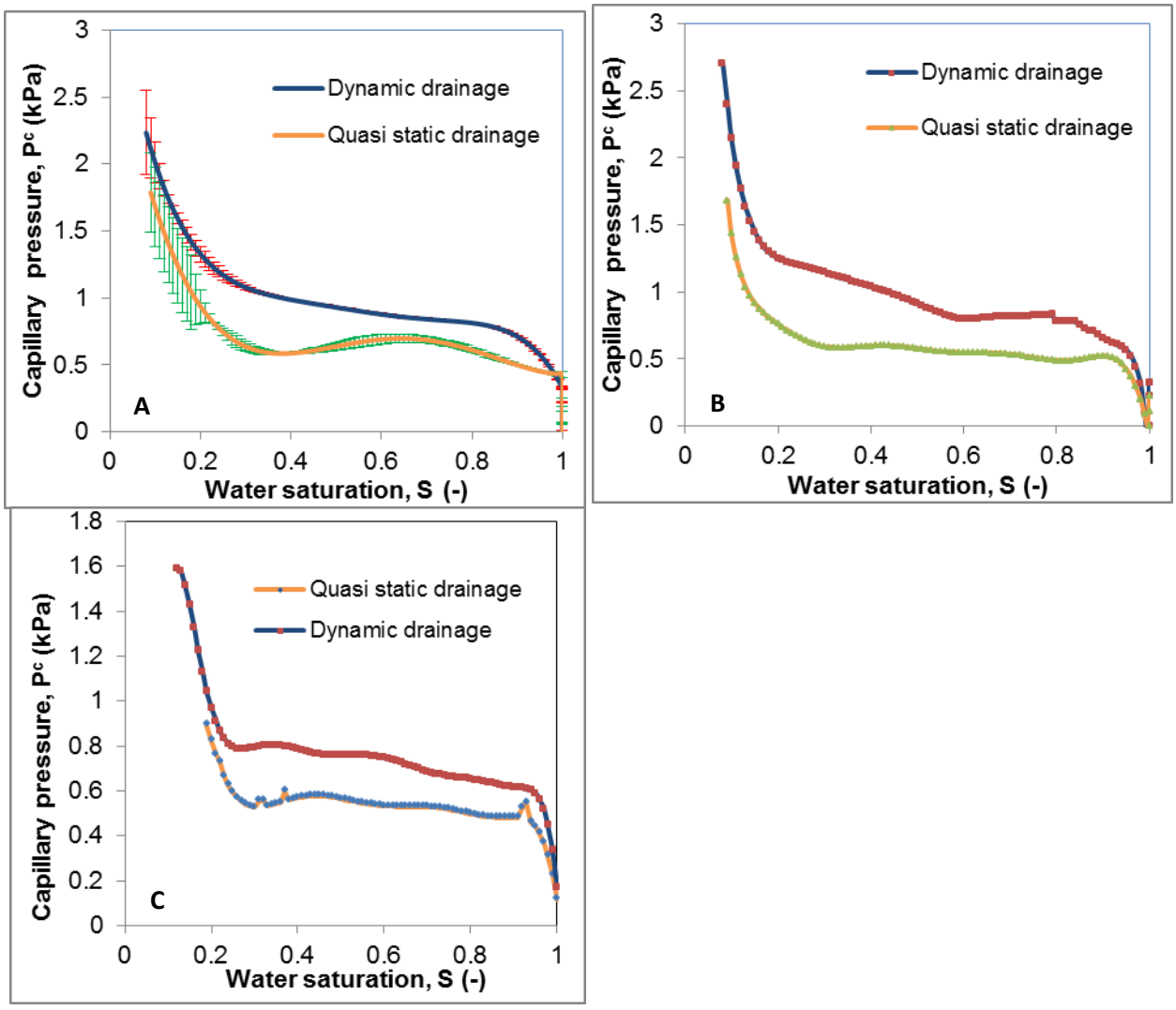

412

413 Figure 2: P^c-S relationship under dynamic and quasi static conditions in (A) coarse sand at
414 40°C, (B) coarse sand at 50°C, (C) coarse sand at 40°C with 0.1% surfactant (by mass).
415 All dynamic experiments are conducted at 80.5 bar.

416 **3.1.2 Displacement pattern in supercritical CO_2–water system in porous media**

417 Data on the desaturation rate ($\partial S/\partial t$) of $scCO_2$-water system in porous media reflects *in*
418 *situ* displacement characteristics of the two-phase system under various conditions.
419 Although the experiments were not specifically designed to understand the stability of
420 displacement front it is known that the stability of the displacement front in CO_2-water
421 system in porous media can determine the extent of the displacement without fingering,
422 which in turn can lead to more storage space (Abidoye et al. 2014; Berg and Ott 2012). On
423 the other hand, unstable displacement can lead to viscous fingering and minimize storage
424 potential of the geological sequestration site.

425 The desaturation rate of the water phase in the domain as the $scCO_2$ is injected is shown
426 in Figure 3 for the coarse sand samples under the same conditions, as in Figure 2. Figure
427 3 shows the desaturation rate in coarse sand at 40°C, 50°C, and in coarse sand sample
428 saturated with 0.1% surfactant solution at 40°C.

429 In the coarse sand saturated with water at 40°C, the figure shows that after a short rise
430 (considering absolute value of $\partial S/\partial t$) in the desaturation rate at the start of the fluid
431 displacement, the $\partial S/\partial t$ becomes virtually constant for wide range of water saturation
432 (between 0.9 and 0.3) until irreducible saturation is approached where the decline in
433 desaturation rate begins. The peak value of $\partial S/\partial t$ (absolute value) in coarse sand at 40°C
434 is found to be around 6.75×10^{-4} s^{-1}. Similar trend as above is exhibited by $\partial S/\partial t$-S
435 relationship in coarse sand at 50°C. The peak of the $\partial S/\partial t$ value occurs around 4.8×10^{-4}
436 s^{-1}, which is lower than in coarse sand at 40°C.

437 The presence of surfactant in the solution is shown to affect the trend in the $\partial S/\partial t$-S profile,
438 as shown in the Figure 3. There is obvious departure from the usual patterns under the
439 influence of surfactant. After the initial short rise, the $\partial S/\partial t$ declines at a fairly constant
440 gradient till irreducible saturation value is attained. The presence of surfactant and the
441 production of foam indeed raises the viscosity of the water and increases its resistance to
442 flow. Thus, the viscosity ratio of the two-phase system ($scCO_2$-water) is reduced by the
443 addition of surfactant. The contact of $scCO_2$ with water/surfactant will also lead to foam
444 production (Ma et al. 2013) and, hence, reduce the mobility of the CO_2 phase (Rafati et al.
445 2012).

446 The $\partial S/\partial t$ values reported in this work are comparable to those reported by Goel and
447 O'Carroll (2011). In silicone oil-water drainage experiments, they reported the highest
448 $\partial S/\partial t$ values of $9.8 \times 10^{-4}$and 2.9×10^{-3} s^{-1} for silicone oil viscosities of 5cSt and 0.65cSt,
449 respectively. In this work, the $\partial S/\partial t$ values range from 4.8×10^{-4} s^{-1} to 6.75×10^{-4} s^{-1} for the
450 coarse sand sample at 50 and 40°C, respectively. The closeness in values of the above
451 results with that of Goel and O'Carroll (2011) can be attributed to the low-viscosity silicone
452 oil used in their experiments. Also, the large portion of the $\partial s/\partial t$-S curve that appears
453 constant for wide range of water saturation can be attributed to the low viscosity ratio
454 between $scCO_2$ and water (i.e., ratio of viscosity of CO_2 to that of water), as well as the
455 high pressure at which the experiments were conducted.

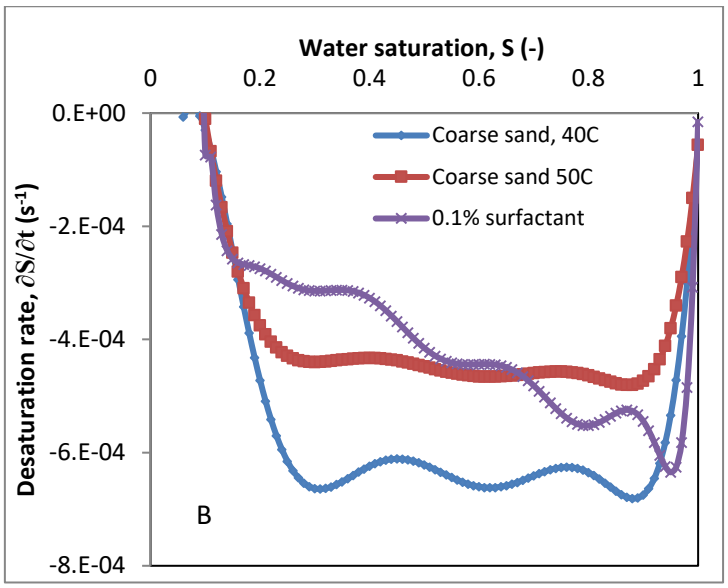

Figure.3: Desaturation rate in coarse sand at 40°C and 50°C, and coarse sand at 40°C saturated with 0.1% surfactant. All dynamic experiments conducted at 80.5 bar.

3.1.3 Dynamic coefficient (τ) for supercritical CO_2-water system in coarse sand sample: Influence of temperature

Dynamic coefficient, τ, have been used to quantify the magnitude of dynamic capillary effects in two-phase flow system (see, e.g., Hassanizadeh and Gray 1990; Hassanizadeh and Gray 1993; Das et al. 2007; Bottero et al. 2011). According to some authors (see, e.g., Hassanizadeh et al., 2002; Das et al., 2007), the dynamic effect is related to the dependence of the P^c-S relationships on the time derivative of saturation resulting from finite time needed by the fluid to neutralise the effect of the internal and external forces in order to establish flow equilibrium. τ establishes the speed at which fluid–fluid interfaces reach equilibrium positions (Das et al. 2007). Thus, a large value of τ indicates a large amount of time for the system to reach equilibrium, while its lower value does otherwise. In this section, we present the results of the calculated dynamic coefficients in $scCO_2$-water system in coarse silica sand sample using equation (2)

The dynamic coefficient, τ, was determined using the data obtained from plots in Figures 2 and 3. The τ-S plots for various conditions in coarse silica sand sample are shown in Figure 4, using semi-log plot. The τ-Scurve rises as the water saturation decreases. The magnitudes of τ under different conditions start with high values at high water saturation. This can be attributed to the low values of ∂S/∂t that is recorded from the start of the desaturation. It is clear from equation (2) that low values of ∂S/∂t lead to high values of τ. In the figure, the magnitudes of τ range from 2.7 x 10^5 Pa s at high water saturation to 7.9

480 x 10^6 Pa s at a saturation close to the irreducible saturation. For low viscosity silicone oil
481 (5cSt) and water system, Goel and O'Carroll (2011) report τ value above 1 x 10^6 Pa s
482 around the start of drainage. In lower viscosity silicone oil (0.65cSt) and water system,
483 value of τ close to 1 x 10^6 Pa s was reported in the region of highwater saturation values.
484 These values of τ from Goel and O'Carroll (2011) are one order of magnitude higher than
485 2.7 x 10^5 Pa s recorded close to the beginning of displacement in this work (Figure 4).
486 Reasons for this may be explained to be due to lower viscosity ratio of the $scCO_2$-water
487 system used in this work compared to the silicone oil-water system used by Goel and
488 O'Carroll (2011). Also, the size of the domain used in their work was higher than the one in
489 this work. It is known that the magnitude of τ increases with increase in viscosity ratio and
490 domain scale (Bottero et al. 2011; Dahle et al. 2005; Goel and O'Carroll 2011; Joekar-
491 Niasar and Hassanizadeh 2011). Similarly, Camps-Roach et al. (2010), using higher
492 domain scale than the one in this work, report values up to 2 x 10^6 Pa s at the start of
493 displacement of water by air in air-water system. However, lower value of τ (less than 5 x
494 10^3 Pa s) is reported around the start of a drainage cycle by Das and Mirzaei (2012) for
495 high viscosity silicone oil (200cSt) and water system.

496 In Figure 4, the values of τ at low values of water saturation appear in the range of 1.3 x
497 10^6 to 8 x 10^6Pa s. This seems to be in agreement with values reported by the above
498 authors. For example, at low water saturation and close to irreducible saturation, Goel and
499 O'Carroll (2011) report values in the range 1 x 10^6Pa s for air-water system, 2 x 10^6 and 3
500 x10^6 Pa s for 0.65 and 5cSt silicone oil, respectively, in silicone oil-water system drainage
501 experiments. Similarly, Das and Mirzaei (2012) report values close to 1 x 10^6 Pa s around
502 irreducible saturation. In Figure 4, the τ-S relationship in the same coarse sand samples
503 are shown for conditions at 40°C, 50°C as well as τ-S relationship in coarse sand
504 saturated with 0.1% surfactant solution at 40°C. The influence of temperature is visible
505 from the τ-S relationship for coarse sand at 50°C which lies higher than at 40°C. This
506 shows that τ increases with temperature. This finding is in conformity with the conclusion
507 of Hanspal and Das (2012). The influence of surfactant on τ-S relationship is not very
508 discernible in the figure as the curve seems to overlie the τ-S curve in coarse sand at
509 40°C.

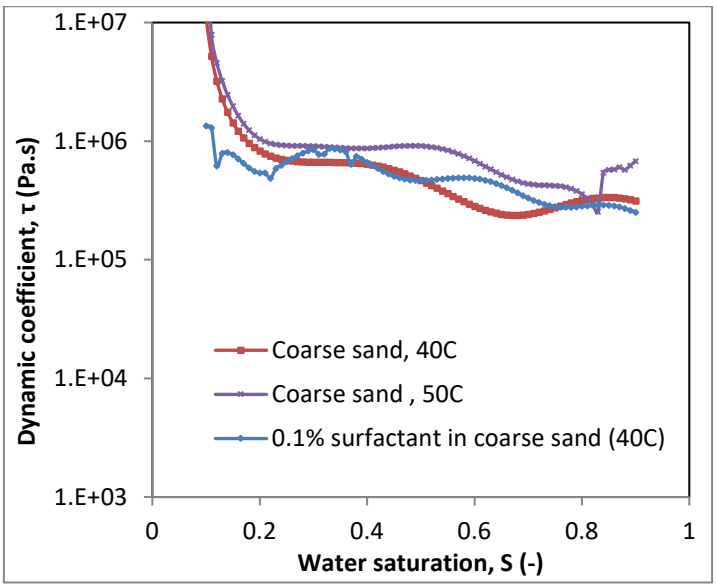

Figure 4: Dynamic coefficients in coarse sand at 40°C, coarse sand at 50°C, and coarse sand saturated with 0.1% surfactant at 40°C. All dynamic experiments conducted at 80.5 bar.

3.1.4 Effect of porous media permeability on τ

It is known that the porous domains in actual sequestration aquifers are characterised with heterogeneity in their properties (e.g., permeability, etc) (Yang et al. 2013; Das et al. 2006; Aggelopoulos andTsakiroglou 2008). Two-phase flow experiments on soils with different properties (e.g., permeabilities, etc.) result in different P^c–S–K_r relationships, i.e., causing non-uniqueness in these curves (Das et al. 2006). Therefore, this section looks into the impact of porous media property, namely, permeability, on τ for $scCO_2$-water system, using finer silica sand (CH30) and the coarser sand (DA14/25). Properties of the two porous media are listed in Table 1.

The P^c-S curves for $scCO_2$-water system in fine silica sand are shown in Figure 5(A). Similar to the behaviour of P^c-S curves shown in Figure 2, the P^c-S relationships remain higher under the dynamic condition as compared to the equilibrium curves. This is an indication of dynamic P^c effect (Das et al. 2014; Khudaida and Das 2014; Abidoye et al.2014; Hassanizadeh and Gray 1990). Comparison of the behaviour of the dynamic P^c-S curves for coarse (DA14/25) and fine (CH30) silica sand is given in Figure 5(B). The figure shows that the P^c-S curve is higher in fine sand than the coarse type. This can be attributed to the increased pore pressure as a result of reduced pore space in the fine sand domain. Similar finding was reported by Das and Mirzaei (2013). They found the P^c-S

534 curve higher in fine sand than the coarse sand. The entry pressure is noticeably higher in
535 fine sand. This can be attributed to the lower permeability of the fine sand sample as
536 shown in Table 1.

537 Low permeability has earlier been identified as one of the factors responsible for higher
538 dynamic effect in porous media (Tian et al. 2012; Das et al. 2007). Figure 5(C) compares
539 the desaturation rate of the water in the porous domains made of finer and coarse silica
540 sand. The figure shows that the desaturation rate (absolute value) is higher in coarse sand
541 than in the fine sand domain. As stated before, this can be attributed to reduced pore
542 space in the fine sand medium, leading to slow movement of fluids. Furthermore, the
543 increase in surface area as a result of the finer grains in the fine sand domain might
544 contribute to the slowing down of the displacement process. The curve follows similar
545 pattern as in the coarse sand sample with short rise in the desaturation rate followed by an
546 almost uniform desaturation rate till saturation value of around 0.3. In the fine sand
547 sample, the average peak in $\partial S/\partial t$ value (absolute) is 2.6 x 10^{-4} (s^{-1}) while the
548 corresponding value in the coarse sand sample is above 6.75 x 10^{-4} (s^{-1}). This shows that
549 displacement of water in the coarse sand sample is faster than in the fine sand. Figure
550 5(D) shows the τ-S relationship in coarse and finer silica sand at 40^{o}C. The figure clearly
551 indicates that the τ-S curve is higher in lower-permeability medium, i.e., higher in fine
552 sand. Thus, going by the interpretation of τ, as explained by Das et al. (2007), it takes
553 longer in fine sand medium to reach the equilibrium than in coarse sand domain.

554

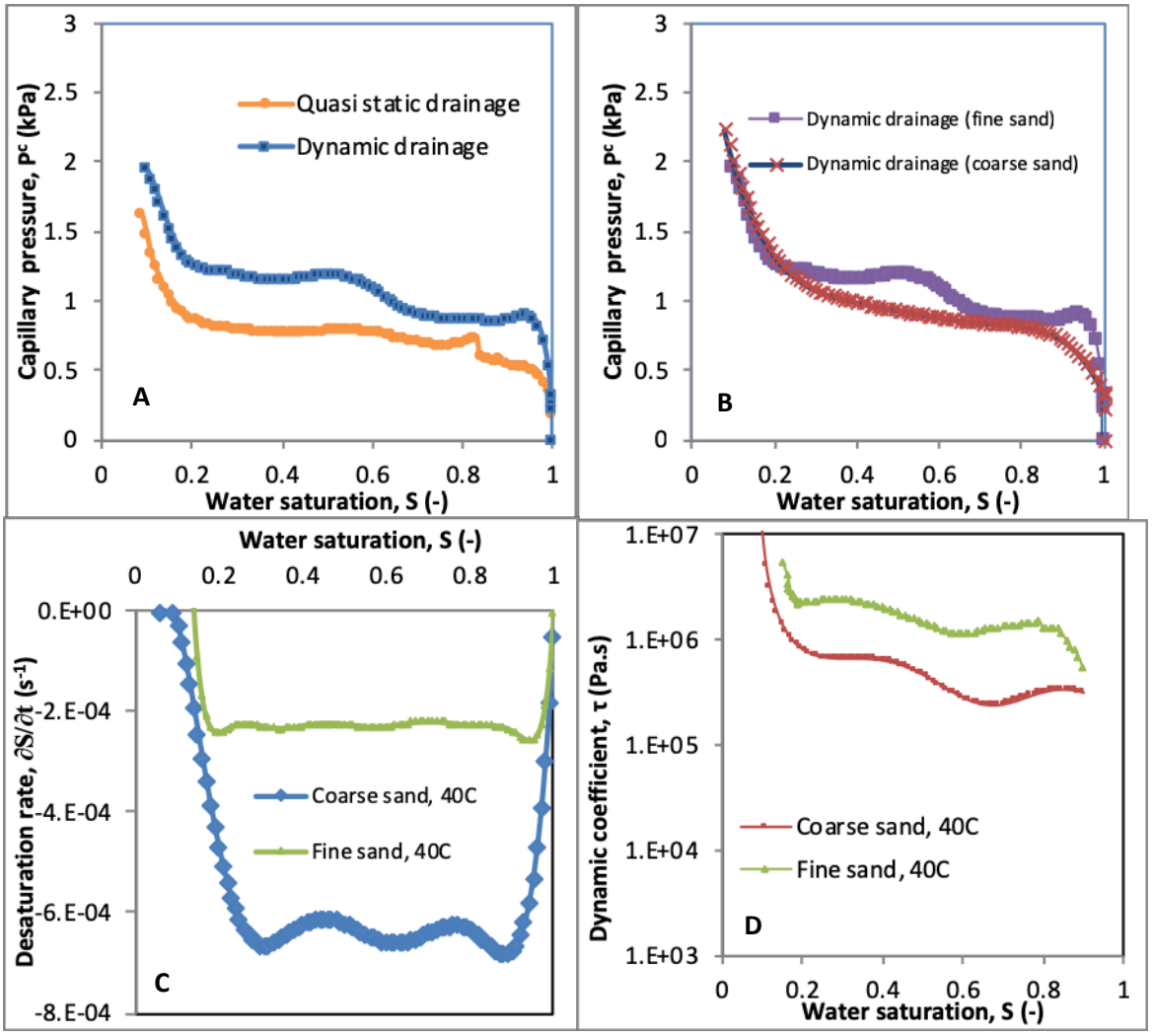

Figure 5: (A) P^c-S relationships for $scCO_2$-water system under dynamic and quasi static conditions in fine sand (CH30) at 40°C, (B) Comparison of dynamic P^c-S relationships for $scCO_2$-water system in coarse and fine silica sand at 40°C, (C) Comparison of desaturation rates in coarse and fine silica sand at 40°C,(D) Comparison of dynamic coefficients in coarse and fine silica sand at 40°C. All dynamic experiments are conducted at 80.5 bar

3.2 Numerical analyses

Numerical simulation was conducted to provide further basis for the results of the experimental investigations discussed in sub-section 3.1 using the simulator STOMP as discussed in sub-section 2.4. This will also affirm how well the experimental measurements discussed above can be placed in the context of known approaches for numerical simulations. However, the simulation does not investigate the influence of

surfactant on the $scCO_2$-water system. Figure6 shows the numerically derived P^c-S curves for material property equivalent tothat of coarse sand (DA 14/25) at different conditions (quasi static and dynamic conditions) and temperatures of 40 and 50^{o}C, respectively. For most of the water saturation, the P^c-S curves in the figure show that the dynamic P^c-S curves lie higher than the P^c-S curve under equilibrium conditions.

The curves in Figure 7 compare numerical simulation results of τ-S relationship with the experimental results in coarse sand at 40 and 50^{o}C. In the figure, it can be appreciated that the numerical τ-S relationship compares well with the corresponding experimental results for wide range of water saturation. Departure of the numerical results from the experimental values only become noticeable at low water saturation values. Comparison of numerical results of τ-S relationships in coarse sand at 40 and 50^{o}C is shown in Figure 7C. The plot shows that the τ-S curve at 50^{o}C lies slightly above the curve at 40^{o}C. This corroborates the experimental findings above which show that the magnitude of τ increases with temperature.

To depict effect of porous media property on τ-S relationships using numerical simulation, the properties of the fine sand (CH30) were used and compared to that of the coarse sand (DA 14/25) that was described earlier (Figures 6 and 7). Figure 8 shows the numerical P^c-S curves in fine sand (CH30) and the comparison of τ-S relationships for fine and coarse sand media. Figure 8B compares numerically simulated and the experimentally determined τ-S relationship in fine sand medium. The plots show that there is a good match between the numerical simulation and experimental results. This confirms the reliability of the experimental findings shown in Figure 5D. Figure 8C shows that the τ-S relationship is higher in fine sand than the coarse type. Hence, with appropriate material characteristics, the τ-S relationship can be successfully investigated with both experiments and numerical simulations.

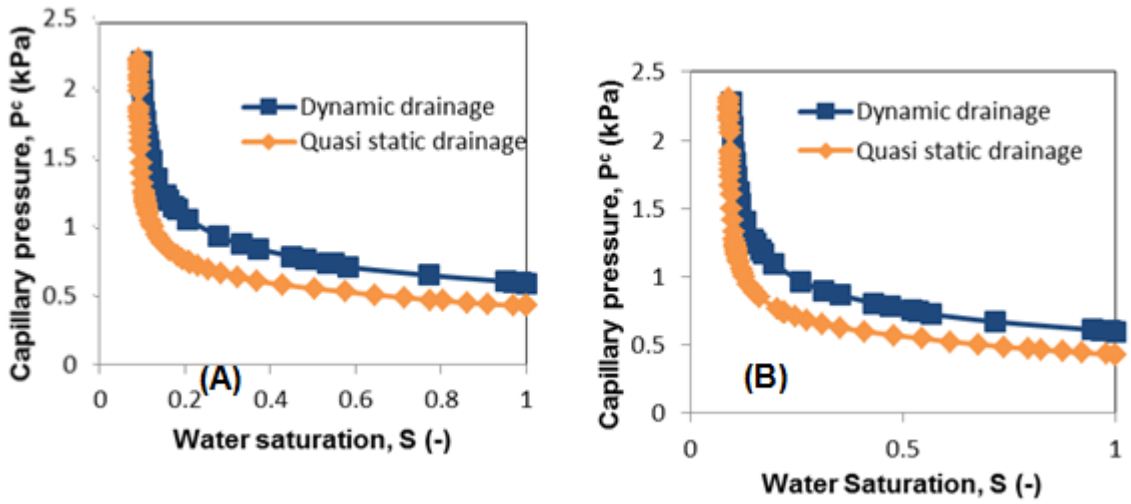

609

610 Figure 6: P^c-S curves from the numerical simulations of the dynamic and quasi static
611 displacements of water by $scCO_2$ in coarse sand medium (A) at 40°C (B) at 50°C.

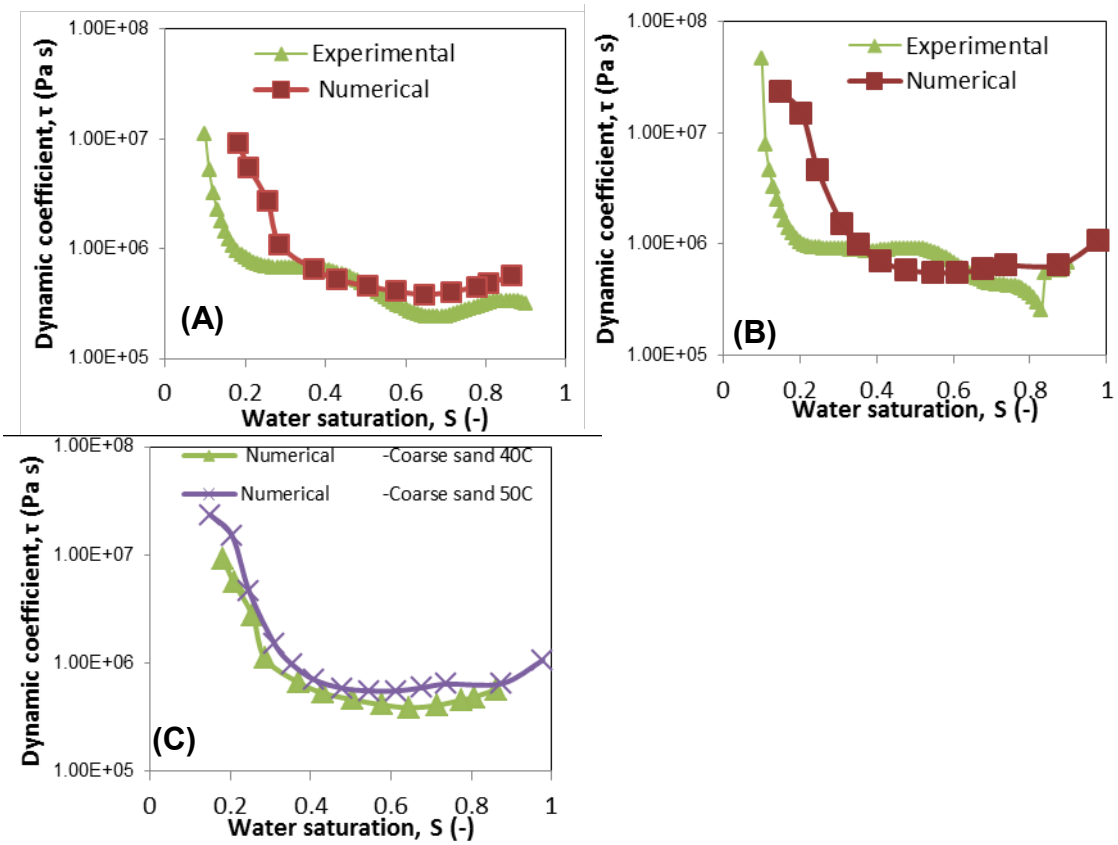

612

613 Figure 7: Numerically and experimentally determined τ-S relationships in coarse sand
614 medium at (A) 40°C (B) 50°C (C) comparison of τ-S at 40 and 50°C. Dynamic
615 experiments and simulations are conducted at 80.5bar.

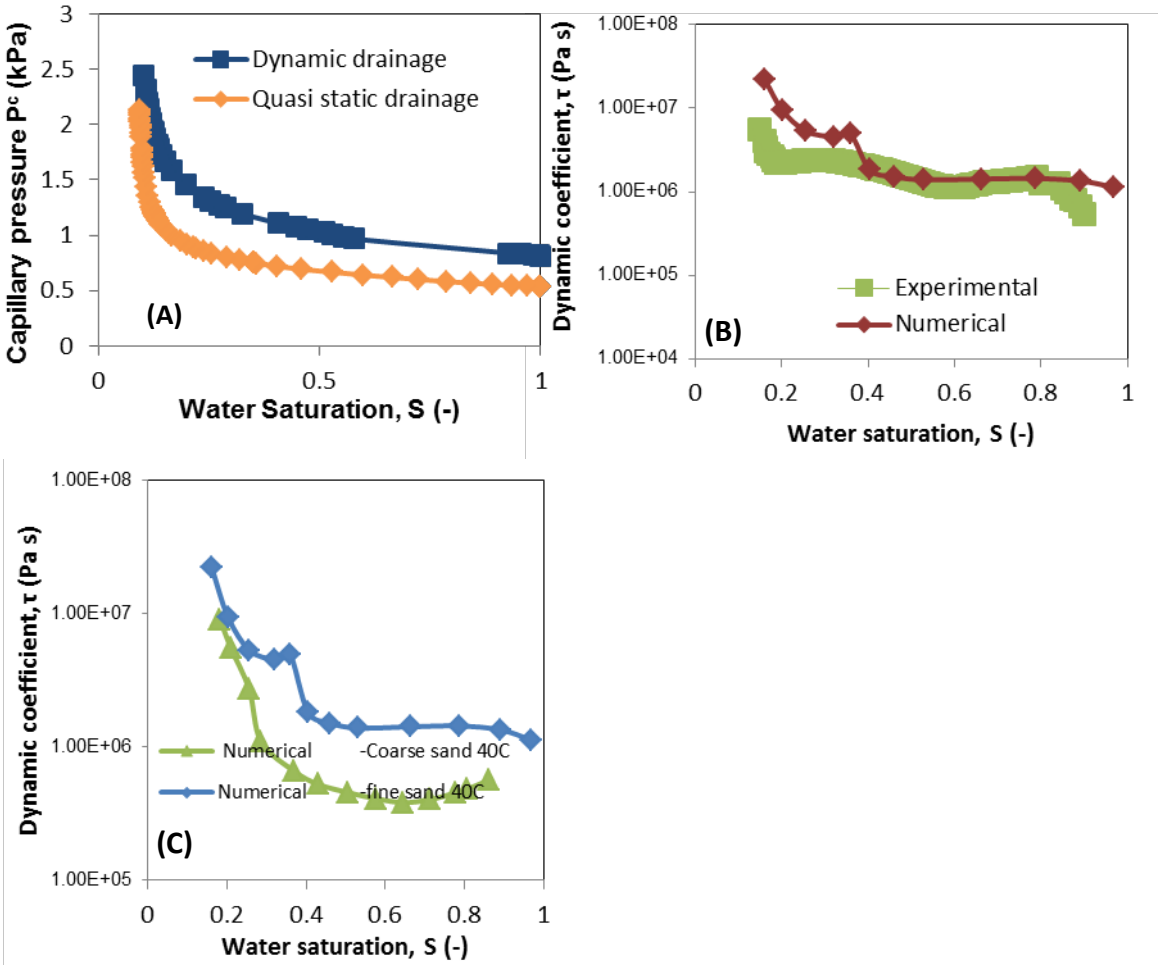

Figure 8: (A) Numerically determined P^c-S relationship in fine sand medium at 40°C (B) Numerically and experimentally determined τ-S relationship in fine sand medium at 40°C (C) Comparison of numerically determined τ-S relationship in fine and coarse sand media at 40°C. Dynamic experiments and simulations conducted at 80.5bar.

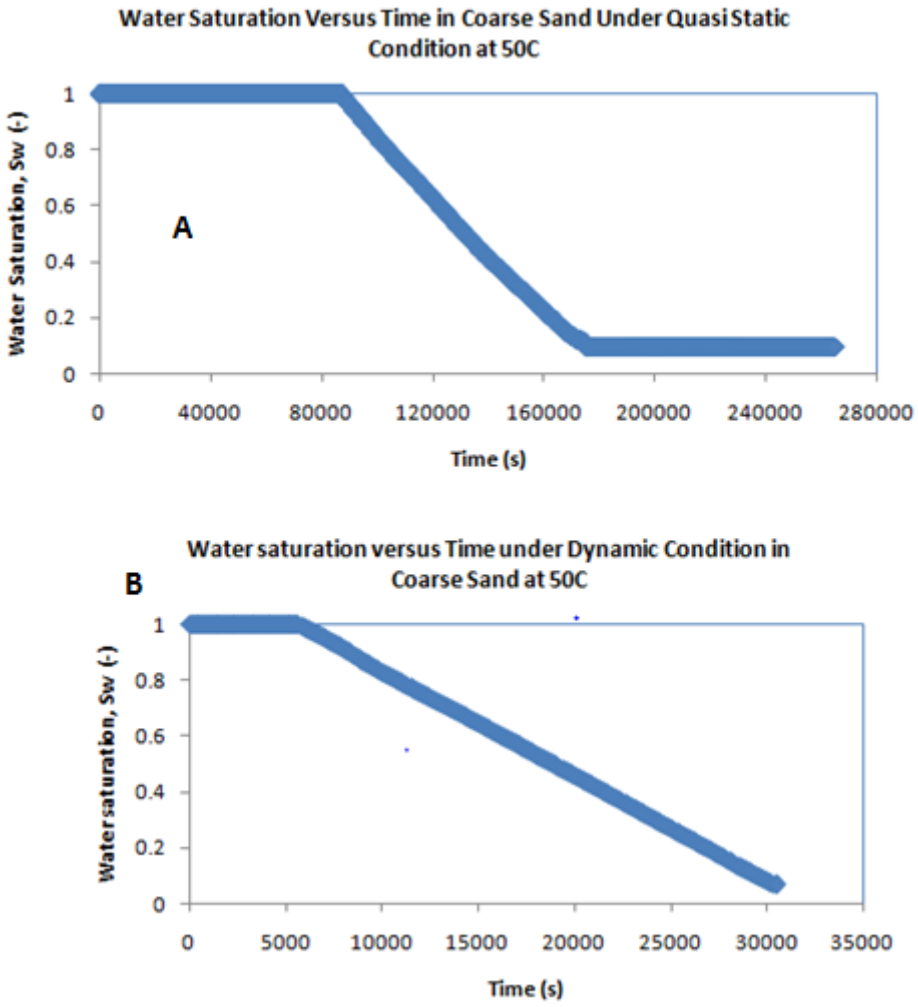

623

624 Figure 9: Saturation-Time Profile in Coarse sand at 50°C (A) Quasi static (B)
625 Dynamic experiments. The plot lines are thick and dense owing to the frequnecy of data
626 acquisitions

627 The profiles of water saturation with time are shown in Figure 9 for the quasi static and
628 dynamic experiments in coarse sand at 50°C.

629 **3.3. Dynamic P^c effects in scCO_2-water system and the impacts on the estimation of**
630 **relative fluid-fluid distribution in porous medium**

631 Capillary pressure and saturation relationship (P^c-S) is useful in the estimation of fluid
632 (e.g., oil and water) distribution in the reservoir (Pini et al. 2012; Benson and Cole 2008;
633 Tokunaga et al. 2013). Since the P^c varies with the change in water saturation, the value of
634 measured P^c gives an indication of the fractional space occupied by the oil/gas and water.
635 In the case of carbon geological sequestration, the measured P^c offers information about
636 the aquifer content of CO_2 and brine/water.

637 As discussed earlier, traditionally, the P^c-S relationship is determined under equilibrium
638 conditions. With dynamic P^c effect, difference/error is introduced into the relationship if

639 applied to two-phase system under flow conditions, i.e., non-equilibrium conditions. In
640 order to illustrate this point further let us consider the equilibrium P^c-S relationship for
641 $scCO_2$-water system in coarse silica sand at 40^{o}C, shown in Figure 2A. Under equilibrium
642 condition, when the P^c of around 0.69 kPa is measured, the domain is about 70% water-
643 saturated. If the $scCO_2$-water is under non-equilibrium condition, a measure of similar
644 magnitude of P^c indicates the domain is about 90% water-saturated. Therefore, if
645 equilibrium P^c-S relationship is applied to the two-phase system, under flow conditions, the
646 porous domain water saturation can be considerably underestimated. This is an
647 implication of the dynamic P^c effect. This difference can affect the judgement of the gas
648 migration in the aquifer as well as the aquifer storage capacity. The difference in the
649 calculation is further magnified by increased temperature. For example, at 50^{o}C (Figure
650 2B), applying the equilibrium P^c-S relationship for measurement at 70% water saturation to
651 the $scCO_2$-water under flow condition introduces higher error to the estimation of the
652 domain water saturation. Furthermore, the effect of permeability raises the
653 underestimation of the domain water saturation at around the same saturation as above.

654 Thus, by using equation (2), the above errors can be eliminated with the knowledge of
655 dynamic coefficient, τ, which correlates the error in the measured P^c to the desaturation
656 rate data. The relation in equation (2) can be used to estimate the expected error under
657 the prevailing desaturation rate value. This can then be applied to quantify the true
658 equilibrium P^c, which can then be used to estimate the actual saturation value of the
659 porous domain.

660 The above results bring to light the fundamental disparity that can be encountered in the
661 application of P^c-S relationship in the study, monitoring, and control of $scCO_2$-water
662 system in the porous media under the dynamic and quasi static conditions. The results are
663 important in the context of geological carbon sequestration. The dynamic effect has been
664 observed in the P^c-S relationship for oil-water and gas-water system (see, references cited
665 above), but little has been reported about the phenomenon for $scCO_2$-water system.
666 Recently, numerical investigations by Khudaida and Das (2014), and Das et al. (2014)
667 show that there is significant dynamic effect in the $scCO_2$-water system. Thus, this work
668 serves as good complimentary experimental confirmation of the phenomenon of dynamic
669 P^c effect and its consequences in the $scCO_2$-water system.

4. Conclusion

The significance of dynamic effects in $scCO_2$-water flow system was investigated by using novel experimental measurement technique together with numerical investigations. For the $scCO_2$-water flow system, the magnitude of saturation rate dependencies of the capillary pressure-saturation (P^c-S) relationship, known as dynamic capillary pressure effect was quantified by dynamic coefficient, τ. Results show that the P^c-S curve under dynamic condition (drainage cycle) lies above the P^c-S curve for the quasi static condition.

τ ranges from 2 $x10^5$ to 6 $x10^5$ Pa s at high water saturation and 1.3 x 10^6 to 8 $x10^6$Pa saround the irreducible saturation. τ increases with rising temperature but decreases with increase in porous medium permeability. Numerically determined τ-S relationships compare well with the corresponding experimental results for wide range of water saturation.

Finally, the errors inherent in the estimation of porous media water saturation as a result of ignoring dynamic P^c effects were evaluated. By ignoring the dynamic capillary pressure effect, the porous media water saturation is underestimated under normal condition. With increased temperature, the error in the estimation of the water saturation increases. With decrease in sample permeability, the degree of underestimation became more pronounced. Clearly, this work shows the importance of accurate determination of fluid distribution in porous media. This can be applicable to geological carbon sequestration, especially during the period of fluid redistribution in the storage aquifer, following the injection of supercritical CO_2.

Acknowledgment

The work is carried out in the framework of EPSRC (UK) project Micro-heterogeneity and Temperature Effects on Dynamic Capillary Pressure-Saturation Relationships for Two-phase Flow in Porous Media (GR/S94315/01).

Data Access

Any data in this paper may be obtained by contacting the corresponding author. The data may also be accessed by accessing Loughborough University institutional repository (http://www.lboro.ac.uk/research/scholcomms/openaccess/lupinir/).

References

Abidoye, L.K. and Das, D.B. (2014).Scale-dependent dynamic capillary pressure effect for two-phase flow in porous media. Advances in Water Resources, 74, pp. 212–230, DOI: 10.1016/j.advwatres.2014.09.009

Abidoye, L.K., Das, D.B., and Khudaida, K., 2014. Geological carbon sequestration in the context of two-phase flow in porous media: A review. Critical Reviews in Environmental Science and Technology, 45(11): 1105-1147, DOI: 10.1080/10643389.2014.924184

Aggelopoulos, C. A. and Tsakiroglou, C.D., 2008. The effect of micro-heterogeneity and capillary number on capillary pressure and relative permeability curves of soils. Geoderma, 148(1), pp.25–34.

Ataie-Ashtiani, B., Hassanizadeh, S M, Oostrom, M., Celia, M A., White, M. D., 2001.Effective parameters for two-phase flow in a porous medium with periodic heterogeneities.Journal of contaminant hydrology, 49(1), pp.87–109.

Barenblatt, G. I., Patzek, T. W., and Silin, D. B. 2003. The Mathematical Model of Nonequilibrium Effects in Water-Oil Displacement. Society of Petroleum Engineers. 8(4),doi:10.2118/87329-PA

Benson, S.M. and Cole, D.R., 2008. CO_2 sequestration in deep sedimentary formations.Elements, 4(5), pp.325–331.

Berg, S. and Ott, H., 2012.Stability of CO_2–brine immiscible displacement.International Journal of Greenhouse Gas Control, 11, pp.188–203.

Bottero, S., Hassanizadeh, S. M., Kleingeld, P. J., Heimovaara, T. J., 2011.Nonequilibrium capillarity effects in two-phase flow through porous media at different scales. Water Resources Research, 47(10), p.W10505.

Brooks, R. and Corey, A., 1964. Hydraulic Properties of Porous Media. Hydrology Papers. Colorado State University.

Burdine, N.T., 1953. Relative permeability calculations from pore size distribution data. Transactions of the American Institute of Mining and Metallurgical Engineers, 198 (1953), pp. 71–78

727 Camps-Roach, G., O'Carroll, D. M., Newson, T. A., Sakaki, T., Illangasekare, T. H., 2010.
728 Experimental investigation of dynamic effects in capillary pressure: Grain size dependency
729 and upscaling. Water Resources Research, 46(8), p.W08544.

730 Chandrappa, R. and Das, Diganta B, 2014. Sustainable Water Engineering: Theory and
731 Practice, John Wiley & Sons.

732 Chandrappa, R., Gupta, S. and Kulshrestha, U.C., 2011.Coping with climate change:
733 principles and Asian context, Springer.ISBN 978-3-642-19674-4.

734 Dahle, H.K., Celia, M. A. and Hassanizadeh, S. M., 2005.Bundle-of-Tubes Model for
735 Calculating Dynamic Effects in the Capillary-Pressure- Saturation Relationship. Transport
736 in Porous Media, 58(1-2), pp.5–22.

737 Danish, M. and Jacquin, C., 1983. Influence du Contraste des Viscositéssur les
738 Perméabilités Relatives lors du Drainage. ExpérimentationetModélisation. Rev. Inst.
739 Franc.Pétrole, 33(6), pp.723–733.

740 Das, D.B., Gill, B. S., Abidoye, L. K., Khudaida, K. J., 2014. A numerical study of dynamic
741 capillary pressure effect for supercritical carbon dioxide-water flow in porous
742 domain.AIChE Journaldoi.wiley.com/10.1002/aic.

743 Das, D.B., Gauldie, R. and Mirzaei, M., 2007. Dynamic Effects for Two-Phase Flow in
744 Porous Media: Fluid Property Effects. AIChE, 53(10), pp.2505–2520.

745 Das, D.B. and Mirzaei, M., 2012. Dynamic effects in capillary pressure relationships for
746 two-phase flow in porous media: Experiments and numerical analyses. AIChE Journal,
747 58(12), pp.3891–3903.

748 Das, D.B. and Mirzaei, M., 2013. Experimental measurement of dynamic effect in capillary
749 pressure relationship for two-phase flow in weakly layered porous media. AIChE Journal,
750 59(5), pp.1723–1734

751 Das, D.B., Mirzaei, M. and Widdows, N., 2006. Non-uniqueness in capillary pressure–
752 saturation–relative permeability relationships for two-phase flow in porous media: Interplay
753 between intensity and distribution of random micro-heterogeneities. Chemical Engineering
754 Science, 61(20), pp.6786–6803.

755 Diamantopoulos, E. and Durner, W., 2012. Dynamic Nonequilibrium of Water Flow in
756 Porous Media: A Review. Vadose Zone Journal, 11(3).

757 Donaldson, E.C., Thomas, R. D., Lorenz, P. B., 1969. Wettability determination and its
758 effect on recovery efficiency.Society of Petroleum Engineers Journal, 9(01), pp.13–20.

759 Donaldson, E.C., Ewall, N. and Singh, B., 1991. Characteristics of capillary pressure
760 curves.Journal of Petroleum Science and Engineering, 6(3), pp.249–261.

761 Dullien, F.A.L. et al., 1990. Can. J.P.T., 29(4), p.63.

762 Elenius, M. and Gasda, S., 2012.Impact of tight horizontal layers on dissolution trapping in
763 geological carbon storage. XIX International Conference on Water Resources CMWR
764 2012, University of Illinois at Urbana-Champaign June 17-22,2012.

765 Goel, G. and O'Carroll, D.M., 2011. Experimental investigation of nonequilibrium capillarity
766 effects: Fluid viscosity effects. Water Resources Research, 47(9), p.W09507.

767 Hanspal, N. and Das, D., 2012. Dynamic effects on capillary pressure–Saturation
768 relationships for two-phase porous flow: Implications of temperature. AIChE Journal, 58(6),
769 pp.1951–1965.

770 Hassanizadeh, S.M., Celia, M.A. and Dahle, H.K., 2002. Dynamic effect in the capillary
771 pressure--saturation relationship and its impacts on unsaturated flow.Vadose Zone
772 Journal, 1(1), pp.38–57.

773 Hassanizadeh, S.M. and Gray, W.G., 1990. Mechanics and thermodynamics of multiphase
774 flow in porous media including interphase boundaries. Advances in water resources, 13(4),
775 pp.169–186.

776 Hassanizadeh, S.M. and Gray, W.G., 1993. Thermodynamic basis of capillary pressure in
777 porous media. Water Resources Research, 29(10), pp.3389–3405.

778 Hou, L., L. Chen, and T. C. G. Kibbey (2012), Dynamic capillary effects in a small-volume
779 unsaturated porous medium: Implications of sensor response and gas pressure gradients
780 for understanding system dependencies, Water Resour. Res., 48, W11522,
781 doi:10.1029/2012WR012434.

782 Jennings, J.B., 1987. Capillary pressure techniques: application to exploration and
783 development geology. AAPG Bulletin, 71(10), pp.1196–1209.

784 Joekar-Niasar, V, Hassanizadeh, SM and Dahle, H.K., 2010. Non-equilibrium effects in
785 capillarity and interfacial area in two-phase flow: dynamic pore-network modelling. Journal
786 of Fluid Mechanics, 655, pp.38-71.

787 Joekar-Niasar, V. and Hassanizadeh, S. M., 2011.Effect of fluids properties on non-
788 equilibrium capillarity effects: Dynamic pore-network modeling. International Journal of
789 Multiphase Flow, 37(2), pp.198–214.

790 Juanes, R., 2008. Nonequilibrium effects in models of three-phase flow in porous media.
791 Advances in Water Resources, 31(4), pp.661–673.

792 Kalaydjian, F., 1992. Effect of the Flow Rate on an Imbibtion Capillary Pressure Curve-
793 Theory Versus Experiment. In SCA European Core Analysis Symposium, Paris, France.

794 Khudaida, K. and Das, D.B., 2014. A numerical study of capillary pressure-saturation
795 relationship for supercritical carbon dioxide (CO_2) injection in deep saline aquifer.
796 Chemical Engineering Research and Design.

797 Lo, W.-C., C.-C. Yang, S.-Y. Hsu, C.-H. Chen, C.-L. Yeh, and M. Hilpert (2017), The
798 dynamic response of the water retention curve in unsaturated soils during drainage to
799 acoustic excitations, Water Resour. Res., 53, 712–725, doi:10.1002/2016WR018833.

800 Ma, K., Lopez-Salinas, J. L., Puerto, M. C., Miller, C. A., Biswal, S. L., Hirasaki, G. J.,
801 2013. Estimation of Parameters for the Simulation of Foam Flow through Porous Media.
802 Part 1: The Dry-Out Effect. doi/abs/10.1021/ef302036s.

803 Mirzaei, M. and Das, D.B., 2007. Dynamic effects in capillary pressure–saturations
804 relationships for two-phase flow in 3D porous media: Implications of micro-heterogeneities.
805 Chemical Engineering Science, 62(7), pp.1927–1947.

806 O'Carroll, D.M., Abriola, L. M., Polityka, C. A., Bradford, S. A., Demond, A. H., 2005.
807 Prediction of two-phase capillary pressure--saturation relationships in fractional wettability
808 systems.Journal of Contaminant Hydrology, 77(4), pp.247–270.

809 O'Carroll, D.M., Phelan, T.J. and Abriola, L.M., 2005. Exploring dynamic effects in capillary
810 pressure in multistep outflow experiments. Water Resour. Res., 41(11), p.W11419.

811 Oung, O., Hassanizadeh, S.M. and Bezuijen, A., 2005. Two-Phase Flow Experiments in a
812 Geocentrifuge and the Significance of Dynamic Capillary Pressure Effect. Journal of
813 Porous Media, 8(3), pp.247–257.

814 Patankar, S., 1980. Numerical heat transfer and fluid flow, CRC Press.

815 Petvipusit, K.R., Elsheikh, A. H., Laforce, T. C., King, P. R., Blunt, M. J., 2014. Robust
816 optimisation of CO2 sequestration strategies under geological uncertainty using adaptive
817 sparse grid surrogates. Computational Geosciences, pp.1–16.

818 Pini, R., Krevor, S.C.M. and Benson, S.M., 2012. Capillary pressure and heterogeneity for
819 the CO2/water system in sandstone rocks at reservoir conditions. Advances in Water
820 Resources, 38, pp.48–59.

821 Plug, W.-J.and Bruining, J., 2007. Capillary pressure for the sand–CO_2–water system
822 under various pressure conditions. Application to CO_2 sequestration. Advances in Water
823 Resources, 30(11), pp.2339–2353.

824 Rafati, R., Hamidi, H. I., Ahmad K. M., Muhammad, A., 2012. Application of sustainable
825 foaming agents to control the mobility of carbon dioxide in enhanced oil recovery. Egyptian
826 Journal of Petroleum, 21(2), pp.155–163.

827 Rosen, M.J., 2004: Reduction of Surface and Interfacial Tension by Surfactants.
828 Surfactants and Interfacial Phenomena, John Wiley and Sons Inc., New York (1995).DOI:
829 10.1002/0471670561.ch5

830 Rudin, J., Bernard, C. and Wasan, D.T., 1994. Effect of added surfactant on Interfacial
831 Tension and Spontaneous Emulsification in Alkali /Acidic Oil Systems. Ind. Eng. Chem.,
832 Res., 33, 1150-1158.

833 Sakaki, T., O'Carroll, D.M. and Illangasekare, T.H., 2010. Direct Quantification of Dynamic
834 Effects in Capillary Pressure for Drainage–Wetting Cycles. Vadose Zone Journal, 9(2),
835 p.424.

836 Stauffer, 1978. Time Dependence of the Relations between Capillary Pressure, Water
837 Content and Conductivity During Drainage of Porous Media. In paper presented at IAHR
838 Symposium on Scale Effects in Porous Media. pp. 766–776.

839 Stephens, J.C., 2006. Growing interest in carbon capture and storage (CCS) for climate
840 change mitigation. Sustainability: Science Practice and Policy, 2(2), pp.4–13.

841 TIAN, S. LEI, G., HE, S., YANG, L., 2012. Dynamic effect of capillary pressure in low
842 permeability reservoirs. Petroleum Exploration and Development, 39(3), pp.405–411.

843 Tokunaga, T.K., Wan, J., Jung., J-W, Kim, T. W., Kim, Y., Deng, W., 2013. Capillary
844 pressure and saturation relations for supercritical CO_2 and brine in sand: High-pressure P
845 c (S_w) controller/meter measurements, and capillary scaling predictions. Water Resources
846 Research. Doi.wiley.com/10.1002/wrcr.20316.

847 Versteeg, H.K. and Malalasekera, W., 1995. An introduction to computational fluid
848 dynamic: The finite volume method, John Wiley and Sons Inc, New York (1995).

849 Wedlake, G.D. and Robinson, D.B., 1979. Solubility of carbon dioxide in silicone
850 oil.Journal of Chemical and Engineering Data, 24(4), pp.305–306.

851 White, M.D., Watson, D.J., Bacon, D.H., White, S.K., McGrail, B.P., Zhang, Z.F., 2012.
852 Subsurface Transport Over Multiple Phases STOMP-CO_2 and -CO_2e Guide, Pacific
853 Northwest National Laboratory. PNNL-21268

854 Wildenschild, D., Hopmans, J.W. and Simunek, J., 2001. Flow rate dependence of soil
855 hydraulic characteristics. Soil Science Society of America Journal, 65(1), pp.35–48.

856 Yang, Z., Zandin, H., Niemi, A., Fagerlund, F., 2013.The role of geological heterogeneity
857 and variability in water infiltration on non-aqueous phase liquid migration. Environmental
858 Earth Sciences, 68(7), pp.2085–2097.

859 Zhuang, L., Hassanizadeh, S. M., Qin, C.-Z., & de Waal, A. (2017). Experimental
860 investigation of hysteretic dynamic capillarity effect in unsaturated flow. Water Resour.
861 Res., 53, 11pp, https://doi.org/10.1002/2017WR020895.

862